[DOI]10.12016/j.issn.2096-1456.202550493

·生物材料专栏 基础研究·

兼具自矿化与成骨诱导特性的六磷酸肌醇-锌水凝胶的制备及性能评价

刘鸣一， 苗晓雨， 蔡云帆， 王妍， 孙小棠， 康靖蕊， 赵耀， 牛丽娜
口颌系统重建与再生全国重点实验室，国家口腔疾病临床医学研究中心，陕西省口腔医学重点实验室，空军军医大学口腔医院修复科，陕西 西安(710032)

【摘要】 目的 构建一种负载六磷酸肌醇-锌的水凝胶，同时初步评估其在自矿化和成骨诱导方面的性能，为骨再生材料开发提供研究基础。**方法** 利用甲基丙烯酰氧乙基三甲基氯化铵(methacryloyloxyethyltrimethylammonium chloride，DMC)和四臂聚乙二醇丙烯酸酯共聚形成水凝胶框架DF_0，再依次借助静电作用和螯合作用负载六磷酸肌醇阴离子和锌离子。仅负载六磷酸肌醇阴离子的水凝胶被命名为DF_1，同时负载六磷酸肌醇-锌的水凝胶被命名为DF_2。通过扫描电镜(scanning electron microscope，SEM)、透射电镜(transmission electron microscope，TEM)、能量色散X射线光谱仪(energy dispersive spectroscopy，EDS)、选区电子衍射(selected area electron diffraction，SAED)等手段表征DF_0、DF_1、DF_2水凝胶自矿化效果；借助死/活细胞染色、CCK-8实验测定DF_0、DF_1、DF_2水凝胶生物相容性；通过碱性磷酸酶(alkaline phosphatase，ALP)和茜素红S(alizarin red S，ARS)染色评估DF_0、DF_1、DF_2水凝胶对小鼠胚胎成骨细胞前体细胞(mouse embryonic osteoblast precursors，MC3T3-E1)的成骨诱导能力；在上述细胞实验中，均以普通培养基饲养的细胞作为对照组。**结果** DF_0、DF_1、DF_2水凝胶被成功合成，其中DF_1、DF_2可在6 d内产生明显的自矿化现象；TEM、EDS、SAED结果证实DF_1组矿化产物为无定形磷酸钙，而DF_2组产物为无定形磷酸锌钙；生物相容性实验结果显示，DF_0、DF_1、DF_2水凝胶未对细胞存活及增殖产生影响；成骨诱导实验中，DF_1组和DF_2组的ALP及ARS染色都有所加深，其中DF_2组两种染色结果最深。**结论** 本研究构建的六磷酸肌醇-锌水凝胶(DF_2)可通过自矿化实现钙磷化合物生成，同时兼具良好的成骨诱导特性；这种生物相容性良好的双重促成骨水凝胶为骨再生提供了一种新的策略。

【关键词】 生物材料； 六磷酸肌醇； 天然化合物； 螯合作用； 锌离子； 自矿化； 成骨诱导； 水凝胶； 骨再生
【中图分类号】 R78 **【文献标志码】** A **【文章编号】** 2096-1456(2026)01-0029-12
【引用著录格式】 刘鸣一，苗晓雨，蔡云帆，等. 兼具自矿化与成骨诱导特性的六磷酸肌醇-锌水凝胶的制备及性能评价[J]. 口腔疾病防治, 2026, 34(1): 29-40. doi:10.12016/j.issn.2096-1456.202550493.

微信公众号

Fabrication and evaluation of an inositol hexaphosphate-zinc hydrogel with dual capabilities of self-mineralization and osteoinduction

LIU Mingyi, MIAO Xiaoyu, CAI Yunfan, WANG Yan, SUN Xiaotang, KANG Jingrui, ZHAO Yao, NIU Lina. State Key Laboratory of Oral & Maxillofacial Reconstruction and Regeneration, National Clinical Research Center for Oral Diseases, Shaanxi Key Laboratory of Stomatology, Department of Prosthodontics, School of Stomatology, The Fourth Military Medical University, Xi'an 710032, China
Corresponding author: NIU Lina, Email: niulina831013@126.com; ZHAO Yao, Email: zy1056314642@foxmail.com

【Abstract】 Objective To fabricate a hydrogel loaded with inositol hexaphosphate-zinc and preliminarily evaluate its performance in self-mineralization and osteoinduction, thereby providing a theoretical basis for the development of bone regeneration materials. **Methods** The hydrogel framework (designated DF_0) was formed by copolymerizing methacryloyloxyethyltrimethylammonium chloride and four-armed poly(ethylene glycol) acrylate, followed by sequentially

【收稿日期】2025-10-29； **【修回日期】**2025-11-26
【基金项目】国家自然科学基金项目(82325012)；中国博士后面上基金项目(2024M754272)
【作者简介】刘鸣一，硕士研究生在读，Email：mingyi-liu@foxmail.com
【通信作者】牛丽娜，教授，博士，Email：niulina831013@126.com；赵耀，助理研究员，博士，Email：zy1056314642@foxmail.com

loading inositol hexaphosphate anions via electrostatic interaction and zinc ions via chelation. The hydrogel loaded only with inositol hexaphosphate anions was named DF_1, while the co-loaded hydrogel was named DF_2. The self-mineralization efficacy of the DF_0, DF_1 and DF_2 hydrogels was characterized using scanning electron microscopy, transmission electron microscopy (TEM), energy dispersive spectroscopy (EDS), and selected area electron diffraction (SAED). The biocompatibility was assessed via live/dead cell staining and a CCK-8 assay. The osteoinductive capacity of the DF_0, DF_1 and DF_2 hydrogels on MC3T3-E1 cells was assessed via alkaline phosphatase (ALP) and Alizarin Red S (ARS) staining. In the aforementioned cell experiments, cells cultured in standard medium served as the control group. **Results** The DF_0, DF_1, and DF_2 hydrogels were successfully synthesized. Notably, DF_1 and DF_2 exhibited distinct self-mineralization within 6 days. Results from TEM, EDS, and SAED confirmed that the mineralization products were amorphous calcium phosphate in group DF_1, and amorphous calciumzinc phosphate in group DF_2. Biocompatibility tests revealed that none of the hydrogels (DF_0, DF_1, and DF_2) adversely affected cell viability or proliferation. In osteogenic induction experiments, both ALP and ARS staining were intensified in the DF_1 and DF_2 groups, with the most profound staining observed in the DF_2 group. **Conclusion** The developed inositol hexaphosphate-zinc hydrogel (DF_2) demonstrates the dual capacity to generate calcium-phosphate compounds through self-mineralization while exhibiting excellent osteoinductive properties. This biocompatible, dual-promoting osteogenic hydrogel presents a novel strategy for bone regeneration.

【Key words】 biomaterial; inositol hexaphosphate; natural compound; chelation; zinc ions; self-mineralization; osteoinduction; hydrogel; bone regeneration

J Prev Treat Stomatol Dis, 2026, 34(1): 29-40.

【Competing interests】 The authors declare no competing interests.

This study was supported by the grants from National Natural Science Foundation of China (No. 82325012) and the China Postdoctoral Science Foundation (No. 2024M754272).

骨是人体内高度矿化的器官之一，其中的坚硬组织部分实际上是骨细胞的外基质，由胶原纤维网络和羟基磷灰石（hydroxyapatite，HAP）组装而成[1]。这些硬组织在体内发挥着重要的支撑、保护作用，与运动、生活息息相关[2]。然而，外伤、衰老等因素相关的骨损伤问题日益严峻，受损骨组织的修复逐渐成为全球性的健康难题[3]。当前，自体骨移植仍然是临床金标准，但此种材料受到来源局限、供骨部位损伤风险等诸多限制[4]。因此，新型生物材料亟待开发，以期促进高质量的骨组织重建。

骨组织的形成是一个多因素协同的复杂过程，既包含钙磷矿物的化学沉积，也受到成骨细胞和破骨细胞等细胞活动的精确调控[5]。基于上述生物学原理，利用生物材料递送骨重建所需原料，或调控骨相关干细胞活性已成为促进骨组织再生的重要策略[6]。在骨原料的选择方面，尽管提供HAP是最直接的策略，然而此种预混晶体往往存在分散不佳、力学不匹配、降解不可控等问题，由此，无定形磷酸钙（amorphous calcium phosphate，ACP）等更具有骨适配性的前驱体化合物逐渐成为研究热点[7]。ACP在促进骨修复方面具有优异的性能，但不稳定性是其突出缺点[8]；针对这一问题，具有高度可设计性的水凝胶材料提供了创新性解决方案；利用水凝胶负载能与钙磷离子发生互作的功能性分子，通过自矿化特性原位生成ACP成为了一种更具应用价值的思路[9]。

六磷酸肌醇是一种富含于植物种子中的天然化合物，单个分子中含有6个磷酸基团，失去质子后形成负电性极强的聚阴离子，可以螯合Ca^{2+}等金属离子，具有通过自矿化制造ACP的潜力[10-11]；此外，其还具有促进干细胞成骨分化的能力[12]。Zn^{2+}作为典型的促成骨金属离子，同样可以被六磷酸肌醇阴离子（inositol hexaphosphate anions，$IP6^{12-}$）螯合，二者可进一步发挥协同成骨潜能[13]。因此，本研究旨在开发一种负载$IP6^{12-}$和Zn^{2+}的水凝胶，该种水凝胶可通过自矿化制造钙磷化合物，并可促进成骨分化，且具有良好的生物相容性，为开发新一代骨修复材料提供了新的策略和研究依据。

1　材料和方法

1.1　材料

甲基丙烯酰氧乙基三甲基氯化铵(methacryloyloxyethyltrimethylammonium chloride, DMC)(M102201,阿拉丁,中国);光引发剂2959(H137984,阿拉丁,中国);四臂聚乙二醇丙烯酸酯(S28943,源叶,中国);六磷酸肌醇钠(S30224,源叶,中国);氯化锌(Z0152,Sigma-Aldrich,美国);模拟体液(simulated body fluid,SBF)(G0390,索莱宝,中国);小鼠胚胎成骨细胞前体细胞(mouse embryonic osteoblast precursor,MC3T3-E1)(CL-0378,普诺赛,中国);碱性磷酸酶(alkaline phosphatase,ALP)染色试剂盒(C3206,碧云天,中国);茜素红S(alizarin red S,ARS)染液(ALIR-10001,赛业,中国);死/活细胞染色试剂盒(C2015S, 碧云天,中国);增强型CCK-8试剂盒(C0041,碧云天,中国);α培养基(PM150421,普诺赛,中国);特级胎牛血清(164210,普诺赛,中国)。

1.2　设备

365 nm手持式光源(EFL-LS-1600-365,EFL,中国);傅里叶变换红外光谱仪(Fourier transform infrared spectroscopy,FTIR)(Spectrum 3,PerkinElmer,美国);扫描电镜(scanning electron microscope,SEM)及其能量色散X射线光谱仪(energy dispersive spectroscopy,EDS)(S-4800,日立,日本);透射电镜(transmission electron microscope,TEM)及其EDS(JEM-F200,JEOL,日本);激光共聚焦显微镜(A1R plus,尼康,日本);电感耦合等离子体质谱(inductively coupled plasma-mass spectrometry,ICP-MS)(iCAP RQ,赛默飞,美国);全波长酶标仪(Multiskan SkyHigh,赛默飞,美国)。

1.3　水凝胶的制备与表征

将8.5%(w/v)DMC、2.5%(w/v)四臂聚乙二醇丙烯酸酯、0.1%(w/v)光引发剂2959充分溶解在去离子水中形成单体溶液,在365 nm光源下固化10 min形成水凝胶,记为DF_0水凝胶。将DF_0水凝胶冻干,利用FTIR检查并比较其与DMC的官能团。

将DF_0水凝胶浸泡于1%(w/v)六磷酸肌醇钠溶液5 min以负载$IP6^{12-}$,制得DF_1;而后将DF_1在0.1 mol/L的氯化锌溶液中浸泡5 min以进一步负载Zn^{2+},所得水凝胶即为DF_2。每次更换浸泡溶液前,使用去离子水充分清洗以去除未负载物质。将DF_0、DF_1、DF_2冻干后,使用SEM选择水凝胶平坦区域,借助EDS元素面扫描模式确定其元素组成(放大倍数×500)。

最后,为评估水凝胶在液体环境中对$IP6^{12-}$及Zn^{2+}的释放,分别称取1 g新鲜的DF_0、DF_1、DF_2水凝胶,置于10 mL生理盐水中,于37 ℃恒温孵箱中孵育。在特定时间点(12 h、1 d、2 d、3 d、4 d)收取上清,使用ICP-MS测定DF_0组、DF_1组、DF_2组上清液中磷元素和锌元素的含量。

1.4　水凝胶的自矿化行为

将DF_0、DF_1、DF_2水凝胶置于15 mL离心管,分别加入3 mL无菌SBF,在37 ℃孵箱中震荡孵育,每隔8 h换液。在1、3、6 d时收集水凝胶块,使用去离子水快速漂洗,拍摄对应时间点DF_0组、DF_1组、DF_2组水凝胶矿化状态,而后冻干并置于SEM下观察(放大倍数×50 000)。

为鉴定水凝胶表面矿化物的成分,将矿化物与水凝胶分离:冻干的水凝胶置于离心管,加入无水乙醇,使用超声破碎15 min,通过低速离心(1 000 r/m,3 min)去除水凝胶沉淀,保留含有矿化物的上清。将上清均匀分散于铜网,在TEM下观察,并使用TEM-EDS确定DF_0组、DF_1组、DF_2组矿化物的元素组成,使用选区电子衍射(selected area electron diffraction,SAED)确定矿化物的结晶状态。

1.5　细胞相容性实验

使用α培养基浸泡DF_0、DF_1、DF_2水凝胶24 h以取得浸提液。取生长状态良好的MC3T3-E1细胞接种于24孔板,每孔2×10^4个细胞。待细胞贴壁后,加入上述浸提液;另保留一组生长状态相同的细胞,加入普通α培养基作为对照组。共培养持续48 h或96 h,随后使用死/活细胞染色试剂盒染色,并迅速置于共聚焦显微镜下观察。

进行CCK-8实验时,MC3T3-E1以3×10^3个/孔的密度接种于96孔板,贴壁后将普通培养基更换为材料浸提液;同样保留一组加入普通α培养基的对照组。在共培养1、3、5 d后取出孔板,在避光条件下加入增强型CCK-8试剂,而后使用酶标仪测定细胞培养孔在450 nm处的吸光度。

1.6　成骨诱导实验

使用成骨诱导培养基浸泡DF_0、DF_1、DF_2水凝胶24 h以取得浸提液。收集MC3T3-E1细胞以α培养基重悬,按1.2×10^4个/孔的密度接种于12孔板。待细胞贴壁后,加入水凝胶成骨诱导培养基浸提液(实验组)或普通成骨诱导培养基(对照组),每隔2~3 d换液。

成骨诱导14 d时,使用多聚甲醛固定细胞

30 min，并使用ALP染色试剂盒避光染色10 min，最后使用蒸馏水充分洗涤以终止反应。

成骨诱导21 d时，在细胞中加入多聚甲醛固定30 min，加入ARS染液室温染色10 min，而后洗去多余染液。在自然光下拍摄ALP和ARS染色结果，并使用Image J对图像进行定量分析。

1.7　统计学方法

所有实验均至少独立重复3次，数据分析借助GraphPad Prism 10.0软件进行。统计学比较使用单因素方差分析和多重比较，结果以平均值±标准差表示。

统计图中星号含义如下：*P< 0.05，**P< 0.01，***P< 0.001，****P < 0.000 1，*ns*=无显著性差异。

2　结　果

2.1　水凝胶的合成与表征

为制备负载六磷酸肌醇-锌的DF_2水凝胶，首先合成无负载的水凝胶DF_0。该水凝胶由DMC和四臂聚乙二醇丙烯酸酯共聚形成，呈高度透明状（图1a）。

利用FTIR检查DMC及DF_0水凝胶中官能团（图1b），在1 637 cm^{-1}处的特征峰归属于C＝C，这一特征峰在DMC单体中存在，而在DF_0水凝胶中消失；位于951 cm^{-1}处的红外特征峰归属于—CH_2—$N^+(CH_3)_3$结构，该特征峰在DMC和DF_0水凝胶中都存在[14-15]。上述结果表明C＝C在聚合反应中被打开，成功交联形成水凝胶网络，而这一过程中季铵基团未被改变。

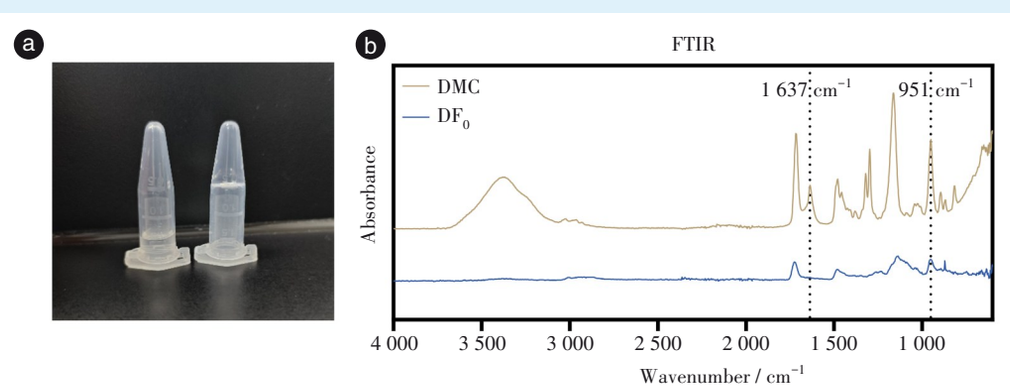

a: photographs of the hydrogel monomer solution before and after photocuring, with the left side taken before 365 nm irradiation and the right side after. b: Fourier transform infrared spectroscopy (FTIR) analysis of the methacryloyloxyethyltrimethylammonium chloride (DMC) and DF_0 hydrogel. The characteristic peak at 1 637 cm^{-1} is attributed to the C=C, which is exclusively present in the DMC monomer. The infrared absorption at 951 cm^{-1} corresponds to the —CH_2—$N^+(CH_3)_3$, and this characteristic peak is observed in both DMC and the DF_0 hydrogel

Figure 1　Synthesis of the DF_0 hydrogel

图1　DF_0水凝胶的合成

EDS检测结果显示（图2），相较于DF_0，DF_1和DF_2水凝胶中依次增加了P和Zn元素的信号峰，证明了$IP6^{12-}$和Zn^{2+}的成功负载。半定量结果显示，DF_1水凝胶中P元素质量占比为6.26%，DF_2水凝胶中P和Zn的元素质量占比分别为4.71%、9.77%。

ICP-MS检测结果显示，DF_1和DF_2组上清中的磷元素含量随着时间升高，提示了这两种水凝胶对$IP6^{12-}$的缓释；释放速度在1 d内相对较快，1 d后有所减缓（图3a）。此外，DF_2水凝胶还能缓释Zn元素，释放规律与P元素相似（图3b）。

2.2　水凝胶的自矿化行为

三种水凝胶在SBF中浸泡后产生了不同的现象。DF_1和DF_2开始逐渐由透明变为白色浑浊，且这种变化具有明显的时间依赖性；与之相反，DF_0水凝胶仍然保持透明（图4）。

将各个时间点的水凝胶收集并冻干，使用SEM观察（图5）。可见未在SBF浸泡时，三种水凝胶表面均平坦无物，在SBF浸泡后，DF_1和DF_2水凝胶表面开始出现球形的沉积物。随时间推移，沉积物数量逐渐增多，6 d时几乎完全覆盖水凝胶表面，这一现象与水凝胶逐渐变浑浊的现象相符。

2.3　水凝胶自矿化产物鉴定

DF_1和DF_2水凝胶表面沉积物被成功分散于铜网，并在TEM下观察。DF_1沉积物颗粒呈现出相对

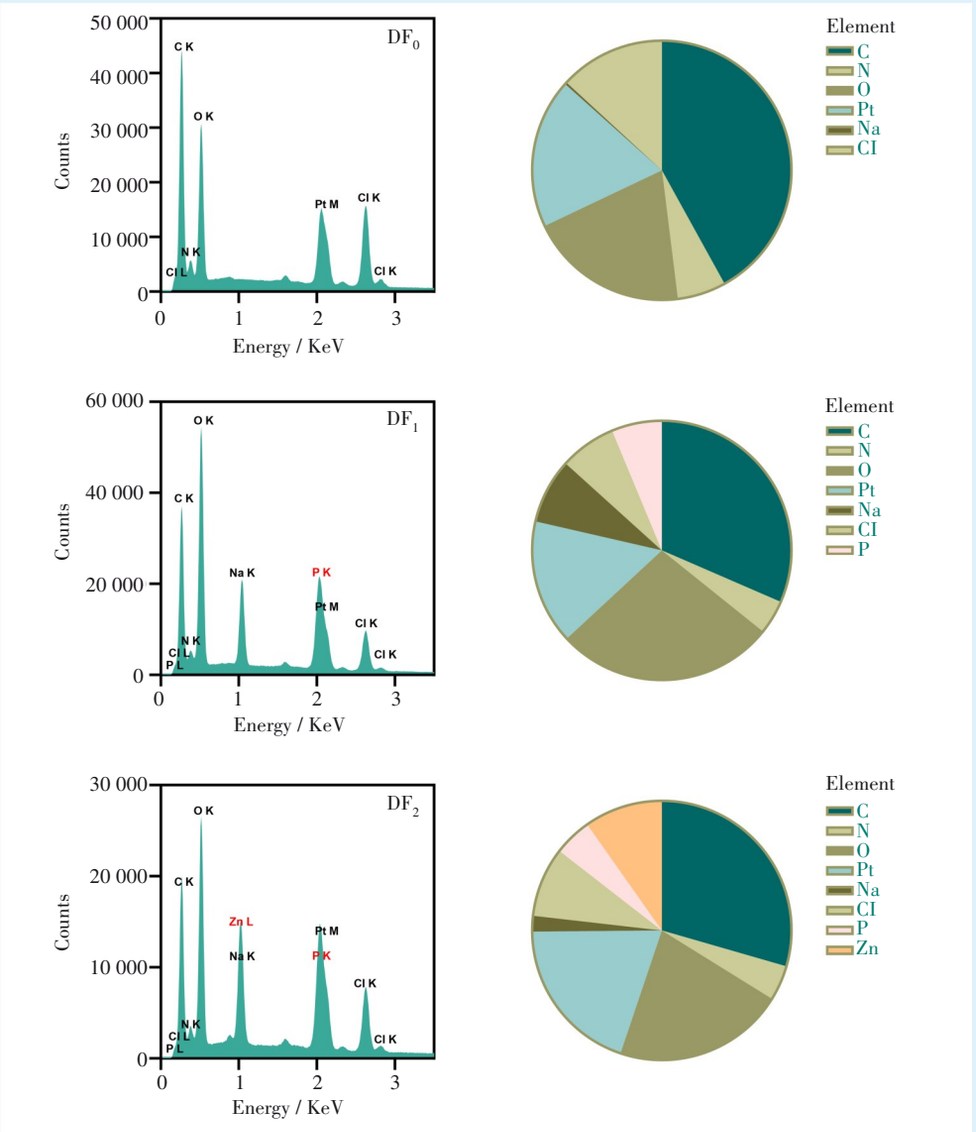

Energy dispersive spectroscopy (EDS) results revealed that no phosphorous (P) or zinc (Zn) elements were detected in the DF_0 hydrogel. The P element began to appear in the DF_1 hydrogel, while both P and Zn were present in the DF_2 hydrogel. DF_0: a monomer solution was prepared by thoroughly dissolving 8.5% (w/v) DMC, 2.5% (w/v) four-armed poly(ethylene glycol) acrylate, and 0.1% (w/v) photoinitiator 2959 in deionized water. The hydrogel formed after curing this solution under 365 nm light for 10 min was designated as DF_0. DF_1: The DF_0 hydrogel was incubated in a 1% (w/v) sodium inositol hexaphosphate solution for 5 min to load $IP6^{12-}$. The resulting hydrogel was labeled DF_1. DF_2: the DF_1 hydrogel was incubated in a 0.1 mol/L Zn chloride solution for 5 min to further load Zn^{2+}. The resulting hydrogel was designated as DF_2

Figure 2　EDS spectra and corresponding elemental mass ratios of the DF_0, DF_1, and DF_2 hydrogels

图2　DF_0、DF_1、DF_2水凝胶的EDS谱图及对应元素质量比

均匀的圆形，分散状态良好（图6a）；DF_2沉积物形态更加细碎，且易于聚集成形态模糊的团簇状（图6b）。对黑色颗粒区域进行SAED，整个衍射图谱中仅有一个明亮的中心斑点，没有任何离散的衍射斑点，提示两种水凝胶表面的沉积物均为无定形物质。

使用TEM-EDS检测上述沉积物的元素组成。结果显示DF_1表面沉积物中主要含有Ca、P、O元素，Ca与P原子比为1.38，结合此前SAED结果，证实其为ACP（图6c）[16-17]。DF_2沉积物除了Ca、P、O元素，还有Zn元素掺杂，Ca与P、Ca与Zn原子比分别为0.44、0.42，为无定形磷酸锌钙（图6d）。EDS谱图中显示的其他元素峰主要来自TEM制样使用的铜网、碳膜，以及残留水凝胶产生的背景。元素面分布图进一步证实了无定形磷酸锌钙的元素聚集情况（图6e）。

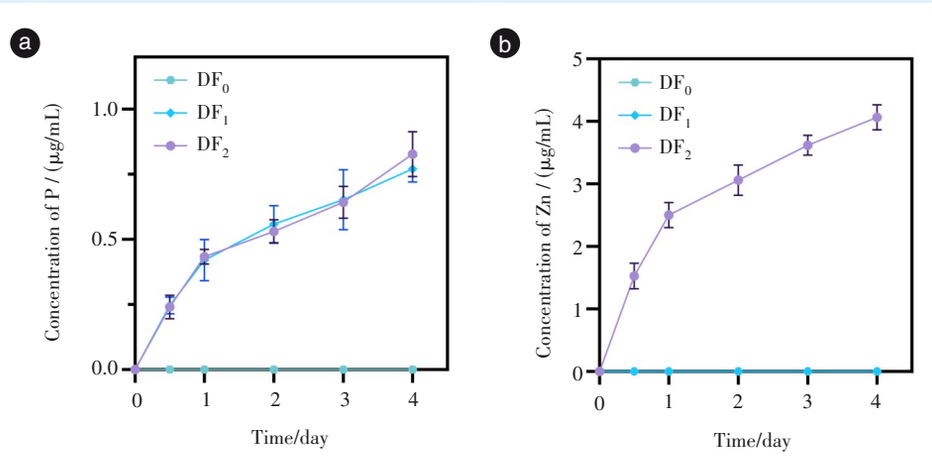

a: release profile of phosphorus (P) from the hydrogels in a liquid environment (n = 3). The gradually increasing concentration of P in the supernatant of the DF_1 and DF_2 groups indicates the sustained release of $IP6^{12-}$. b: release profile of zinc (Zn) from the hydrogels in a liquid environment (n = 3). The progressively rising Zn content in the supernatant of DF_2 groups suggests the sustained release of Zn^{2+}. DF_0 group: normal saline incubated with DF_0 hydrogel. DF_1 group: normal saline incubated with DF_1 hydrogel. DF_2 group: normal saline incubated with DF_2 hydrogel

Figure 3　Phosphorus and zinc release profiles of the DF_0, DF_1, and DF_2 hydrogels

图3　DF_0、DF_1、DF_2水凝胶的磷、锌元素释放曲线

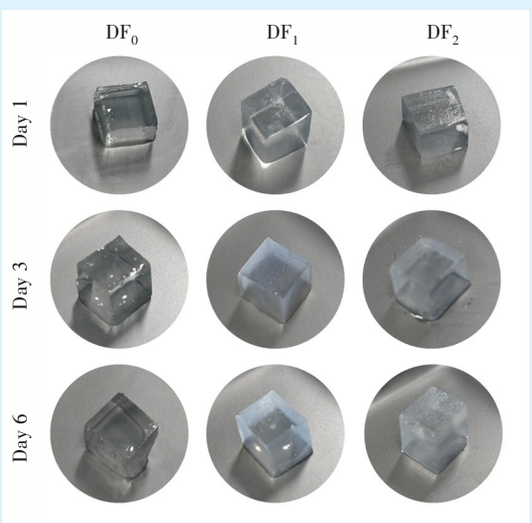

With prolonged incubation in simulated body fluid (SBF), the DF_1 and DF_2 hydrogels gradually transitioned from transparent to turbid, while the DF_0 hydrogel remained transparent even after 6 days of incubation. DF_0 group: DF_0 hydrogels after incubation in SBF for 1, 3, and 6 days. DF_1 group: DF_1 hydrogels after incubation in SBF for 1, 3, and 6 days. DF_2 group: DF_2 hydrogels after incubation in SBF for 1, 3, and 6 days

Figure 4　Photographs of the DF_0, DF_1, and DF_2 hydrogels after immersion in SBF

图4　DF_0、DF_1、DF_2水凝胶在SBF浸泡后的照片

2.4　水凝胶的生物相容性

使用激光共聚焦显微镜观察死/活细胞染色结果，DF_0、DF_1、DF_2组镜下均充满代表活细胞的绿色荧光，仅有零星死细胞的红色荧光（图7a）。CCK-8法检测结果显示，加入3种水凝胶浸提液的细胞培养孔在450 nm处的OD值与对照组无显著性差异（图7b）。上述实验表明3种水凝胶皆未影响细胞存活及增殖，未对细胞产生毒害作用。这种良好的生物相容性为后续成骨诱导实验奠定基础。

2.5　水凝胶的成骨诱导性能

将DF_0、DF_1、DF_2水凝胶浸提液与MC3T3-E1细胞共培养，使用ARS和ALP染色法检测其成骨诱导效果。

14 d时，DF_0水凝胶组的染色效果与对照相比未有变化，而DF_1和DF_2组ALP染色加深，其中DF_2组最深，提示了成骨诱导程度的逐步提高。

21 d时，ARS的染色结果呈现出与ALP相似的趋势：DF_0水凝胶未能提高钙结节数量，DF_1组有所提高，DF_2组钙结节最多，ARS染色颜色最红。利用ImageJ软件对ALP和ARS染色结果进行半定量，统计结果与肉眼观察到的趋势一致（图8）。

3　讨　论

DMC分子结构中含有1个碳碳双键，在交联剂和光引发剂存在的情况下极易发生自由基聚合[18-19]；而四臂聚乙二醇丙烯酸酯分子中含4个碳碳双键，在作为水凝胶单体的同时也可以有效充当交联剂，因此本研究中报道的水凝胶体系可以

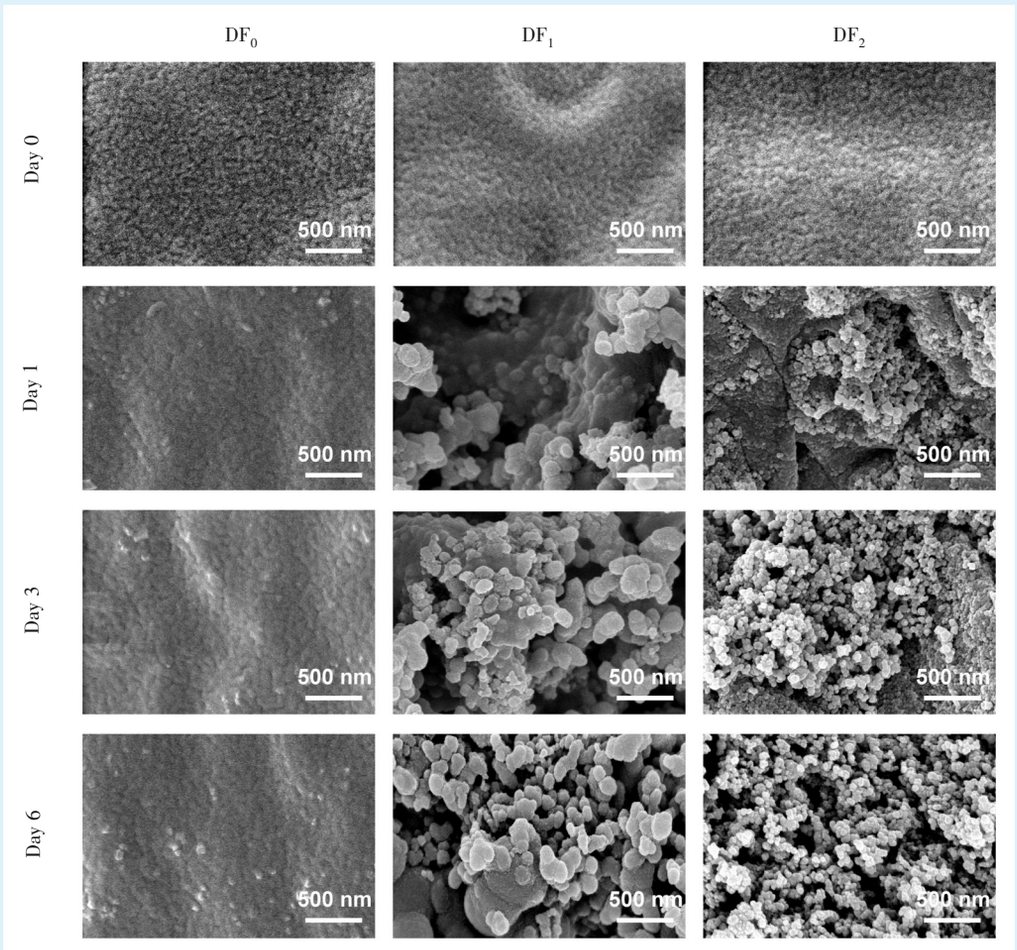

Scanning electron microscope (SEM) results showed that spherical deposits emerged on the surfaces of the DF_1 and DF_2 hydrogels after simulated body fluid (SBF) immersion, and their abundance increased with prolonged immersion time. DF_0 group: DF_0 hydrogels immersed in SBF and lyophilized. DF_1 group: DF_1 hydrogels immersed in SBF and lyophilized. DF_2 group: DF_2 hydrogels immersed in SBF and lyophilized

Figure 5　SEM images of the DF_0, DF_1, and DF_2 hydrogels before and after immersion in SBF

图5　DF_0、DF_1、DF_2水凝胶在SBF浸泡前后的SEM图像

在365 nm光照下，在10 min内轻松地由液体固化形成DF_0水凝胶，具有极高可加工性[20]。通过控制固化条件，这种光引发体系还有望形成膜、微球等更多形态，为其在骨膜修复、骨填充微球等更广泛的骨组织工程场景中的应用奠定了坚实基础，体现了该体系巨大的通用潜力[21-22]。

课题组利用$IP6^{12-}$天然的负电特性和独特的螯合特性，构建了一种分步、可控的负载与矿化系统。$IP6^{12-}$是天然的聚负电离子，其通过静电作用与DF_0水凝胶中悬垂的带正电的季铵基团相结合，因而得以在水凝胶中实现负载，形成DF_1[23]。随后，借助$IP6^{12-}$对金属离子的螯合作用，DF_1进一步负载Zn^{2+}，以形成DF_2水凝胶[24]。DF_1、DF_2水凝胶的自矿化能力也同样归因于$IP6^{12-}$的螯合作用[25]。在DF_1水凝胶的矿化过程中，SBF中的Ca^{2+}首先被螯合于DF_1水凝胶表面，致使表面微环境中的Ca^{2+}浓度提高，从而促使Ca、P元素在水凝胶表面沉积形成ACP[26]。DF_2水凝胶矿化过程与之类似，尽管$IP6^{12-}$已经部分螯合了Zn^{2+}，但由于SBF环境中Ca^{2+}丰富，水凝胶表面Ca的聚集仍然可以通过Ca^{2+}与Zn^{2+}之间的离子交换实现[27]，最后促进Ca、P、Zn共沉积形成无定形磷酸锌钙。

在ACP中，这种金属离子的掺杂是可被接受的，因为人体中的ACP也往往掺杂了其他离子[28-29]。有研究表明锌掺杂的ACP除了作为成骨原料，还可发挥抗炎等额外功能[30]。此外，由于$IP6^{12-}$对其他金属离子，如Fe^{3+}、Mn^{2+}、Mg^{2+}、Cu^{2+}等也普遍具有螯合作用[31-33]，这种广谱螯合能力预示本

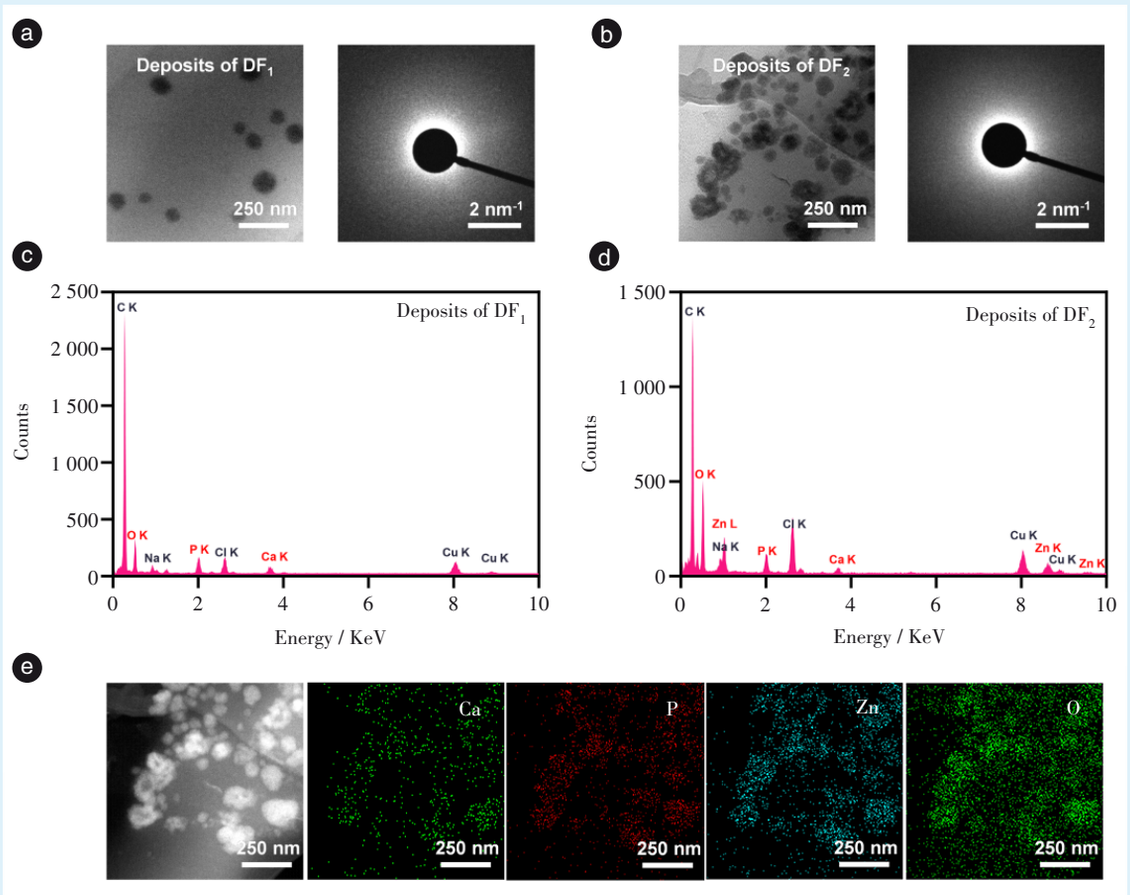

a: transmission electron microscope (TEM) image and corresponding selected area electron diffraction (SAED) pattern of the deposits separated from the DF_1 hydrogel. The SAED results indicated that they are amorphous materials. b: TEM image and corresponding SAED pattern of the deposits separated from the DF_2 hydrogel. The SAED results indicated that they are amorphous materials. c: energy dispersive spectroscopy (EDS) spectrum of the deposits separated from the DF_1 hydrogel. d: EDS spectrum of the deposits separated from the DF_2 hydrogel. e: elemental mapping of the deposits separated from the DF_2 hydrogel. These deposits exhibited distinct colocalization of calcium (Ca), phosphorous (P), zinc (Zn), and oxygen (O). Deposits of the DF_1 group: deposits derived from the mineralization of the DF_1 hydrogel in simulated body fluid (SBF). Deposits of the DF_2 group: deposits derived from the mineralization of the DF_2 hydrogel in SBF

Figure 6　Characterization of self-mineralization products in the hydrogels

图6　水凝胶自矿化产物鉴定

平台技术具有极高的可扩展性；利用六磷酸肌醇金属盐的自矿化能力，生产掺杂金属离子的ACP的思路可能成为一种通用策略[34]。例如，通过负载Mg^{2+}或Cu^{2+}，该体系或可被设计为兼具促血管化或抗菌功能的下一代骨修复材料[35-36]。

近年来，已有多种基于有机分子的自矿化水凝胶被开发用于骨修复，但本研究构建的水凝胶在矿化条件和效率上展现出独特的优势：在矿化条件方面，许多优秀的矿化体系需要施加较高浓度的钙磷溶液才能有效引发矿化[37]；相比之下，本研究的水凝胶在正常浓度的模拟体液（1×SBF）中即可实现矿化，这种条件更接近于生理环境，预示着其在实际应用中具有更佳的临床应用潜力。另外，在矿化效率方面，与依赖柠檬酸等小分子调控的自矿化水凝胶相比，基于$IP6^{12-}$的水凝胶自矿化效率更高，这一差异主要源于$IP6^{12-}$提供了远超柠檬酸的负电荷密度及钙离子螯合能力，从而能更有效地在水凝胶体系中诱导钙磷沉积[9]。因此，本研究通过在水凝胶中引入$IP6^{12-}$这一新颖策略，克服了现有体系在矿化条件或动力学方面面临的部分挑战。

体外细胞毒性实验证实了所有水凝胶均无明显细胞毒性，这一发现与前人研究结论相符：$IP6^{12-}$作为从植物中提取的天然产物，是一种已被广泛

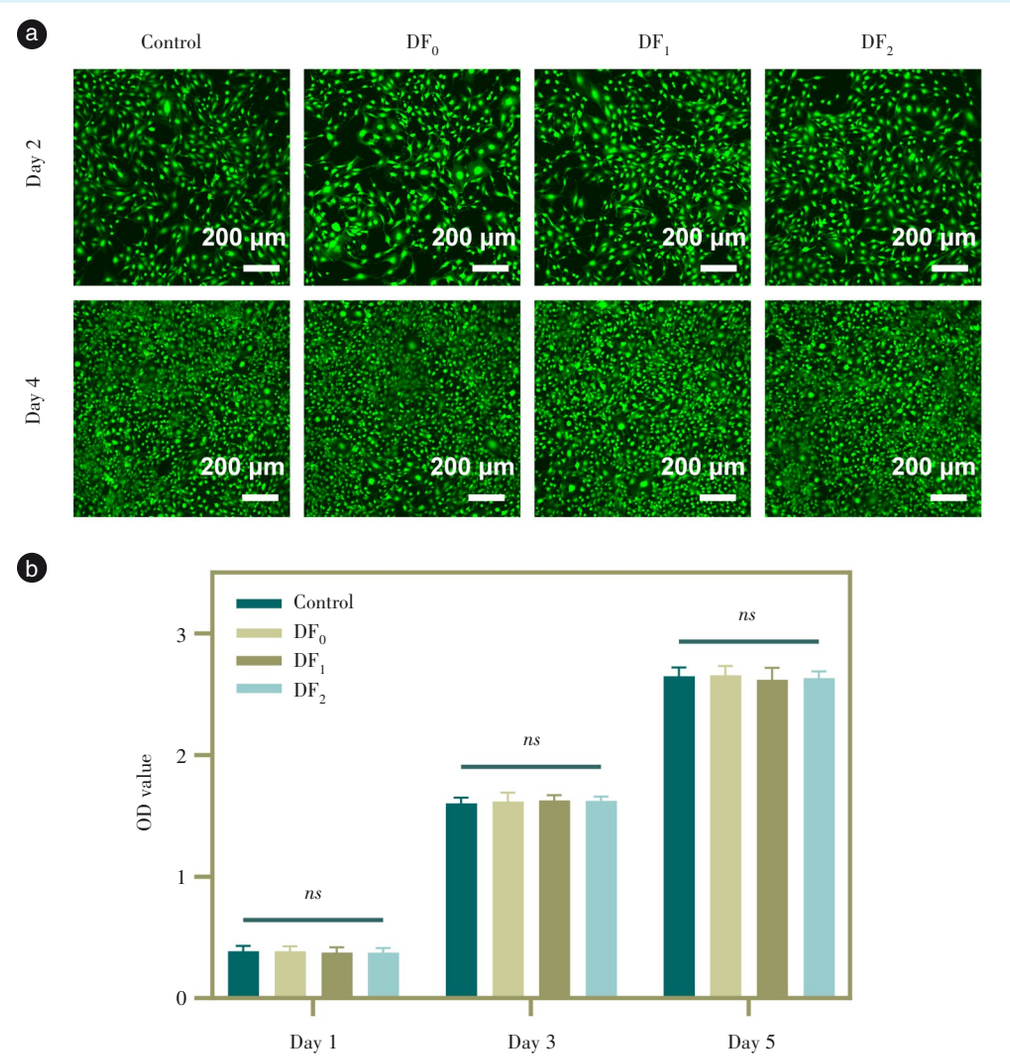

a: fluorescence images of dead/live staining of MC3T3-E1 cells. The viability of cells from the DF_0, DF_1, and DF_2 groups was comparable to that of the control group. b: absorbance at 450 nm of cell culture wells after adding CCK-8 reagent (n = 3). *ns* = not significant. No significant differences in absorbance were observed among all the groups on days 1, 3, and 5. Control group: MC3T3-E1 cells cultured in standard α-MEM medium. DF_0 group: MC3T3-E1 cells cultured in α-MEM medium containing extracts from the DF_0 hydrogel. DF_1 group: MC3T3-E1 cells cultured in α-MEM medium containing extracts from the DF_1 hydrogel. DF_2 group: MC3T3-E1 cells cultured in α-MEM medium containing extracts from the DF_2 hydrogel

Figure 7　Biocompatibility assessment of the DF_0, DF_1, and DF_2 hydrogels

图7　DF_0、DF_1、DF_2水凝胶的生物相容性检测

使用的食品添加剂[38]，Zn也是人体固有的金属元素之一，二者良好的生物安全性均已得到广泛报道[39-40]。这种良好的细胞相容性为本材料的临床转化提供了重要的安全性依据。

本研究最核心的发现在于，DF_2水凝胶兼顾了生物活性矿化与化学成骨信号的双重功能，除了通过自矿化制造成骨原料，还能主动调控细胞成骨分化行为，实现了从被动修复到主动诱导的升级[41]。正如细胞成骨诱导实验所示，DF_1（水凝胶负载$IP6^{12-}$）的浸提液已能体现出一定的成骨诱导效果，而DF_2（水凝胶同时负载$IP6^{12-}$与Zn^{2+}）的浸提液在促进成骨分化方面表现最优，其ALP活性及钙结节形成数量均显著高于DF_1组。上述结果与$IP6^{12-}$及Zn^{2+}固有的成骨诱导活性相关。有研究表明，$IP6^{12-}$的成骨诱导作用依赖磷酸化细胞外调节蛋白激酶（ERK）等通路，其与Zn^{2+}的成骨诱导作用可能起到协同作用[42-43]。

综上所述，本研究成功开发了一种基于$IP6^{12-}$

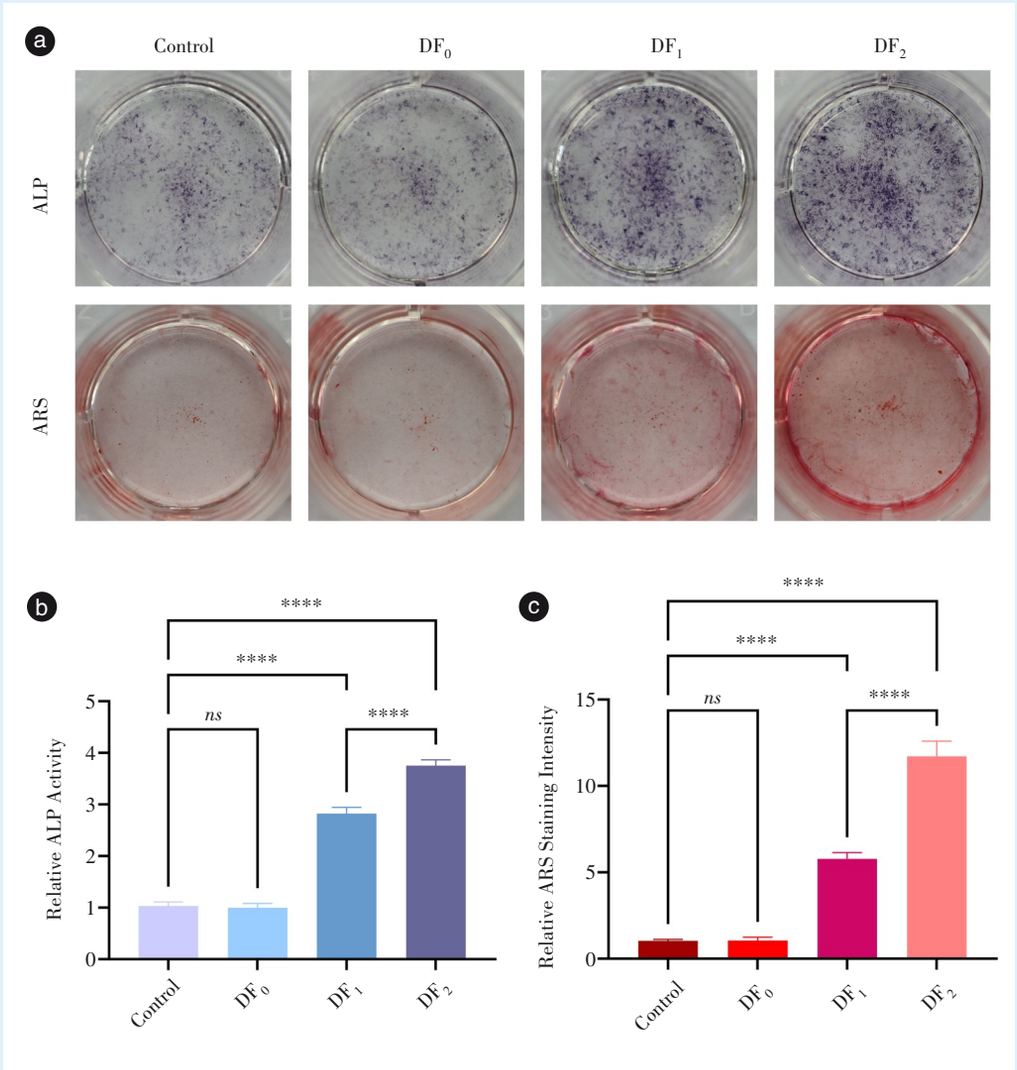

a: alkaline phosphatase (ALP) and alizarin red S (ARS) staining results of mouse embryonic osteoblast precursors (MC3T3-E1). The expression of ALP (14 d) and the number of calcium nodules (21 d) were elevated in the DF_1 and DF_2 groups, with the most pronounced enhancement observed in the DF_2 group. b: semi-quantitative analysis of ALP staining (n = 3). c: semi-quantitative analysis of ARS staining (n = 3). $^{****}P < 0.000\ 1$, *ns* = not significant. Control group: MC3T3-E1 cells cultured in standard osteogenic induction medium. DF_0 group: MC3T3-E1 cells cultured in osteogenic induction medium containing extracts from the DF_0 hydrogel. DF_1 group: MC3T3-E1 cells cultured in osteogenic induction medium containing extracts from the DF_1 hydrogel. DF_2 group: MC3T3-E1 cells cultured in osteogenic induction medium containing extracts from the DF_2 hydrogel

Figure 8　Evaluation of the osteogenic induction capacity of the DF_0, DF_1, and DF_2 hydrogel extracts

图8　DF_0、DF_1、DF_2水凝胶浸提液成骨诱导性能测定

与Zn^{2+}互作的多功能水凝胶DF_2。尽管本研究目前仍停留在体外表征与细胞水平验证阶段，但结果已充分证明该体系集光固化可加工性、可控自矿化能力与协同成骨诱导活性于一身，并且具有良好的生物相容性。这种水凝胶有望为骨修复提供新的思路，应用前景广阔。诚然，该材料在复杂体内环境中的实际修复效能尚不明确，这是本研究当前的主要局限性。因此，未来的研究工作将明确地围绕体内实验展开：一是在动物模型中验证其原位修复骨缺损的卓越疗效；二是基于本文提出的通用策略，探索该平台负载其他功能金属离子在骨组织工程中更广泛的应用；三是进一步设计、开发和体内验证基于该化合物体系的更多材料形式，从而确保该体系能在骨组织工程中发挥最佳治疗效果。

【Author contributions】 Liu MY performed the experiments and wrote the article. Miao XY, Cai YF, Wang Y, Sun XT and Kang JR

were responsible for data analysis. Zhao Y, Niu LN designed the study and revised the article. All authors read and approved the final manuscript submitted.

参考文献

[1] Li Z, Du T, Ruan C, et al. Bioinspired mineralized collagen scaffolds for bone tissue engineering[J]. Bioact Mater, 2021, 6(5): 1491-1511. doi: 10.1016/j.bioactmat.2020.11.004.

[2] Cavalcante RC, Yang X, Xiu K, et al. Nanofibrous scaffolds for bone and cartilage regeneration[J]. Appl Phys Rev, 2025, 12(3): 031319. doi: 10.1063/5.0225639.

[3] Hoenig T, Ackerman KE, Beck BR, et al. Bone stress injuries[J]. Nat Rev Dis Primers, 2022, 8(1): 26. doi: 10.1038/s41572-022-00352-y.

[4] Robin M, Mouloungui E, Castillo Dali G, et al. Mineralized collagen plywood contributes to bone autograft performance[J]. Nature, 2024, 636(8041): 100-107. doi: 10.1038/s41586-024-08208-z.

[5] Lecka-Czernik B, Rosen CJ, Napoli N. The role of bone in whole-body energy metabolism[J]. Nat Rev Endocrinol, 2025, 21(12): 743-756. doi: 10.1038/s41574-025-01162-4.

[6] Xu J, Vecstaudza J, Wesdorp MA, et al. Incorporating strontium enriched amorphous calcium phosphate granules in collagen/collagen-magnesium-hydroxyapatite osteochondral scaffolds improves subchondral bone repair[J]. Mater Today Bio, 2024, 25: 100959. doi: 10.1016/j.mtbio.2024.100959.

[7] Yun J, Woo HT, Lee S, et al. Visible light-induced simultaneous bioactive amorphous calcium phosphate mineralization and *in situ* crosslinking of coacervate-based injectable underwater adhesive hydrogels for enhanced bone regeneration[J]. Biomaterials, 2025, 315: 122948. doi: 10.1016/j.biomaterials.2024.122948.

[8] Zhang Y, Liu Z, Zhang W, et al. Non-collagenous protein-inspired hydrogels with repeated dicarboxylic structure and high matrix strength for amorphous calcium phosphate stabilization to promote bone defect regeneration[J]. Adv Funct Mater, 2025, 35(27): 2500075. doi: 10.1002/adfm.202500075.

[9] Sánchez-Ferrero A, Mata Á, Mateos-Timoneda MA, et al. Development of tailored and self-mineralizing citric acid-crosslinked hydrogels for *in situ* bone regeneration[J]. Biomaterials, 2015, 68: 42-53. doi: 10.1016/j.biomaterials.2015.07.062.

[10] 吴小玉, 汪涛, 周苗, 等. 植酸/氢氧化钙改性对3D打印纯钛多孔结构生物矿化的影响[J]. 稀有金属, 2020, 44(7): 680-686. doi: 10.13373/j.cnki.cjrm.xy18120025.
Wu XY, Wang T, Zhou M, et al. Phytic acid/hydroxide hydroxide surface modification on biomineralization properties of 3D printed porous titanium[J]. Chin J Rare Met, 2020, 44(7): 680-686. doi: 10.13373/j.cnki.cjrm.xy18120025.

[11] Kumar A, Singh B, Raigond P, et al. Phytic acid: blessing in disguise, a prime compound required for both plant and human nutrition[J]. Food Res Int, 2021, 142: 110193. doi: 10.1016/j.foodres.2021.110193.

[12] Wu J, Li X, Nie H, et al. Phytic acid promotes high glucose-mediated bone marrow mesenchymal stem cells osteogenesis *via* modulating circEIF4B that sponges miR-186-5p and complexes with IGF_2BP_3[J]. Biochem Pharmacol, 2024, 222: 116118. doi: 10.1016/j.bcp.2024.116118.

[13] Yan F, Yu M, He Y, et al. Hierarchical mineralized collagen coated Zn membrane to tailor cell microenvironment for guided bone regeneration[J]. Adv Funct Mater, 2025, 35(7): 2412695. doi: 10.1002/adfm.202412695.

[14] Li S, Zhi L, Chen Q, et al. Reversibly adhesive, anti-swelling, and antibacterial hydrogels for tooth-extraction wound healing[J]. Adv Healthc Mater, 2024, 13(14): e2400089. doi: 10.1002/adhm.202400089.

[15] He P, Wang D, Zheng R, et al. An antibacterial biologic patch based on bacterial cellulose for repair of infected hernias[J]. Carbohydr Polym, 2024, 333: 121942. doi: 10.1016/j. carbpol.2024.121942.

[16] Shah FA. Revisiting the physical and chemical nature of the mineral component of bone[J]. Acta Biomater, 2025, 196: 1-16. doi: 10.1016/j.actbio.2025.01.055.

[17] King JMD, D'Amaral MC, Ogata AF. Role of heterogeneous enzyme activity in the formation of calcium phosphate nanomaterials [J]. Nano Lett, 2025, 25(13): 5124-5131. doi: 10.1021/acs.nanolett.4c05766.

[18] Luo J, Shen Z, Jian W, et al. A facile strategy to fabricate stretchable, low hysteresis and adhesive zwitterionic elastomers by concentration-induced polymerization for wound healing[J]. Chem Eng J, 2024, 496: 153804. doi: 10.1016/j.cej.2024.153804.

[19] Ming A, Li X, Sun J, et al. The comparison of polymerization activity of typical cationic quaternary ammonium salt monomers[J]. Polym Adv Technol, 2024, 35(1): e6277. doi: 10.1002/pat.6277.

[20] Miar S, Gonzales G, Dion G, et al. Electrospun composite-coated endotracheal tubes with controlled siRNA and drug delivery to lubricate and minimize upper airway injury[J]. Biomaterials, 2024, 309: 122602. doi: 10.1016/j.biomaterials.2024.122602.

[21] Wang Z, Li X, Jiang Y, et al. Preparation of hydrogel microsphere and its application in articular cartilage injury[J]. Mater Today Bio, 2025, 31: 101641. doi: 10.1016/j.mtbio.2025.101641.

[22] Yin J, Yu L, Zhao R, et al. A photocurable elastic polyester-based Janus bio-adhesive for press-induced *in situ* wound closure[J]. Adv Funct Mater, 2025, 35(42): 2506173. doi: 10.1002/adfm.202506173.

[23] Jiang Y, He X, Xiang L, et al. Phytic acid-polypeptide network-promoted deposition of photoactive agents for the construction of synergistic bactericidal coatings[J]. ACS Appl Mater Interfaces, 2025, 17(24): 36260-36272. doi: 10.1021/acsami.5c09482.

[24] Yan Z, Luo F, Yang S, et al. Polydentate ligand-induced surface reconstruction of MIL-88A reinforced gel electrolytes for highly reversible zinc batteries *via* ion rectification and charge redistribution[J]. Adv Funct Mater, 2025. doi: 10.1002/adfm.202514679.

[25] Amat T, Assifaoui A, Buczkowski J, et al. Formation of insoluble complexes upon calcium addition to total pea globulins or isolated 7S and 11S fractions: impact of pH and intrinsic phytic acid content[J]. Food Hydrocoll, 2025, 168: 111560. doi: 10.1016/j.foodhyd.2025.111560.

[26] Shi J, Feng Y, Zhang S, et al. Intracellular small molecule/ion

storm from Ca-phytate nanoparticle synergizes neural stem cell therapy and immunomodulation in spinal cord injury[J]. Biomaterials, 2026, 326: 123708. doi: 10.1016/j.biomaterials.2025.123708.

[27] Stanimirova T. Exchange reactions of zinc hydroxide-sulfate minerals in halide solutions[J]. Appl Clay Sci, 2019, 168: 396-408. doi: 10.1016/j.clay.2018.12.010.

[28] Kim JY, Kumar SB, Park CH, et al. Development of cell-laden photopolymerized constructs with bioactive amorphous calcium magnesium phosphate for bone tissue regeneration *via* 3D bioprinting[J]. Int J Biol Macromol, 2024, 267(Pt 2): 131412. doi: 10.1016/j.ijbiomac.2024.131412.

[29] Ressler A, Ivanković T, Ivanišević I, et al. Multiphase zinc and magnesium mono-substituted calcium phosphates derived from cuttlefish bone: a multifunctional biomaterials[J]. Ceram Int, 2023, 49(7): 11005-11017. doi: 10.1016/j.ceramint.2022.11.295.

[30] Wang S, Huang C, Zhang X, et al. Zinc doped amorphous calcium phosphate integrated GBR module role in facilitating bone augmentation *via* immunostimulation of osteogenesis[J]. J Mater Sci Technol, 2025, 226: 320-333. doi: 10.1016/j.jmst.2024.12.014.

[31] Yang Y, Li J, Qiao W, et al. Defect-rich birnessite ultrathin nanosheet array armed with Fe-phytate complex enables boosted and long-lasting seawater oxidation at industrial-level current density[J]. ACS Catal, 2025, 15(9): 6954-6968. doi: 10.1021/acscatal.5c00581.

[32] Gong Z, Xiao T, Wu D, et al. Injectable plant phosphate coordination compound-based adhesive hydrogel accelerates osteoporotic fracture healing by restoring osteoclast/osteoblast imbalance[J]. ACS Nano, 2025, 19(37): 33601-33619. doi: 10.1021/acsnano.5c11716.

[33] Zhao Z, Chen H, Zhang H, et al. Polyacrylamide-phytic acid-polydopamine conducting porous hydrogel for rapid detection and removal of copper (II) ions[J]. Biosens Bioelectron, 2017, 91: 306-312. doi: 10.1016/j.bios.2016.12.047.

[34] Wang J, Wang X, Xu D. Machine learning insights into calcium phosphate nucleation and aggregation[J]. Acta Biomater, 2025, 195: 547-558. doi: 10.1016/j.actbio.2025.02.036.

[35] 王天琦, 杜青, 谢伟丽. 钛表面微弧氧化-微波水热法铜铌涂层的制备及抗菌性研究[J]. 口腔疾病防治, 2021, 29(11): 733-739. doi: 10.12016/j.issn.2096-1456.2021.11.002.
Wang TQ, Du Q, Xie WL. Preparation and antibacterial properties of a copper-niobium coating on a titanium surface by a microarc oxidation-microwave hydrothermal method[J]. J Prev Treat Stomatol Dis, 2021, 29(11): 733-739. doi: 10.12016/j.issn.2096-1456.2021.11.002.

[36] Wang Y, Wang X, Pang Y, et al. Ion-engineered microcryogels *via* osteogenesis-angiogenesis coupling and inflammation reversing augment vascularized bone regeneration[J]. Adv Funct Mater, 2024, 34(34): 2400745. doi: 10.1002/adfm.202400745.

[37] 王岩松, 刘建林, 陈晓霞, 等. Exendin4-PEGDA/HA矿化水凝胶的制备及体外成骨作用的研究[J]. 口腔医学研究, 2020, 36(8): 731-735. doi: 10.13701/j.cnki.kqyxyj.2020.08.007.
Wang YS, Liu JL, Chen XX, et al. Preparation and *in vitro* osteogenesis of Exendin4-PEGDA/HA mineralized hydrogel[J]. J Oral Sci Res, 2020, 36(8): 731-735. doi: 10.13701/j.cnki.kqyxyj.2020.08.007.

[38] Li B, Zhou Y, Wen L, et al. The occurrence, role, and management strategies for phytic acid in foods[J]. Compr Rev Food Sci Food Saf, 2024, 23(5): e13416. doi: 10.1111/1541-4337.13416.

[39] Yu SY, Wu T, Xu KH, et al. 3D bioprinted biomimetic MOF-functionalized hydrogel scaffolds for bone regeneration: synergistic osteogenesis and osteoimmunomodulation[J]. Mater Today Bio, 2025, 32: 101740. doi: 10.1016/j.mtbio.2025.101740.

[40] Hsu Y, He Y, Zhao X, et al. Photothermal coating on zinc alloy for controlled biodegradation and improved osseointegration[J]. Adv Sci (Weinh), 2025, 12(9): e2409051. doi: 10.1002/advs.202409051.

[41] Li Y, Ji L, Yu J, et al. Bioactive materials-mediated regulation of bone marrow microenvironment: mechanistic insights and therapeutic potentials[J]. Adv Mater, 2025. doi: 10.1002/adma.202511497.

[42] Liu DY, Wu J, Zhou HY, et al. Phytic acid improves osteogenesis and inhibits the senescence of human bone marrow mesenchymal stem cells under high-glucose conditions *via* the ERK pathway[J]. Chem Biol Interact, 2024, 387: 110818. doi: 10.1016/j.cbi.2023.110818.

[43] Chen J, Chen J, Zhu Z, et al. Drug-loaded and anisotropic wood-derived hydrogel periosteum with super antibacterial, anti-inflammatory, and osteogenic activities[J]. ACS Appl Mater Interfaces, 2022, 14(45): 50485-50498. doi: 10.1021/acsami.2c12147.

（编辑　张琳）

官网